https://doi.org/10.5194/egusphere-2026-4387
Preprint. Discussion started: 17 August 2026

Impacts of ozone-vegetation feedbacks on surface ozone in a coupled climate-chemistry-ecosystem model

Yuan Zhao[1], Weijie Fu[1], Chenguang Tian[1], Jingchao Huang[1], Yihan Hu[1], Xu Yue[1*]

[1] State Key Laboratory of Climate System Prediction and Risk Management (CPRM), Jiangsu Collaborative Innovation Center of Atmospheric Environment and Equipment Technology, School of Environmental Science and Engineering, Nanjing University of Information Science & Technology (NUIST), Nanjing, 210044, China

Corresponding author: Xu Yue (Email: yuexu@nuist.edu.cn)

https://doi.org/10.5194/egusphere-2026-4387
Preprint. Discussion started: 17 August 2026

Abstract

Surface ozone (O_3) is strongly influenced by interactions between atmospheric chemistry and terrestrial ecosystems, yet these feedbacks remain insufficiently represented in Earth system models. Here, we develop a fully coupled O_3-vegetation interaction framework by integrating the terrestrial ecosystem model iMAPLE into the ECHAM-HAMMOZ Earth system model. The coupled model explicitly represents three major land-atmosphere interaction pathways, including dynamic biogenic volatile organic compound (BVOC) emissions, vegetation-mediated O_3 dry deposition, and O_3-induced vegetation damage. These feedback pathways exert heterogeneous impacts on surface O_3 concentrations due to spatial variations in vegetation characteristics and nonlinear chemical sensitivities. Changes in monoterpene emissions cause the largest global effect with widespread reductions in surface O_3, whereas isoprene-driven responses vary among regions with different chemical sensitivities. In regions with high anthropogenic emissions, such as East Asia, vegetation-mediated changes in BVOCs and dry deposition substantially amplify O_3 responses. The O_3-induced vegetation damage further modifies atmospheric chemistry by reducing BVOC emissions through leaf area loss while increasing surface O_3 by inhibiting stomatal conductance. Incorporating these processes decreases simulated global surface O_3 concentrations and alleviates the positive bias in the original model, particularly over China (relative mean bias decreases from 31.5% to 29.7%) and the U.S. (from 19.0% to 7.8%). These results demonstrate that interactive O_3-vegetation feedbacks are essential for improving the representation of atmospheric composition and ecosystem–atmosphere interactions in Earth system models.

Keywords: iMAPLE, ozone-vegetation interactions, ecosystems, atmospheric chemistry

https://doi.org/10.5194/egusphere-2026-4387
Preprint. Discussion started: 17 August 2026

1. Introduction

Tropospheric ozone (O_3) is an important secondary air pollutant and short-lived climate forcer that plays a central role in atmospheric oxidation chemistry (Stevenson et al., 2013; Monks et al., 2015; Ipcc, 2021). Elevated surface O_3 concentrations threaten human health, reduce crop yields, and impair terrestrial ecosystem productivity (Anenberg et al., 2010; Tai et al., 2014; Mills et al., 2018). In the atmosphere, O_3 influences the lifetime of methane and other reactive trace gases, thereby affecting radiative forcing and climate (Fiore et al., 2002; Young et al., 2013; Ipcc, 2021). Over recent decades, surface O_3 pollution has intensified in many regions, particularly in eastern Asia, making it a key challenge at the intersection of air quality, climate change, and ecosystem functioning (Cooper et al., 2014; Gaudel et al., 2018; Lu et al., 2018).

Terrestrial vegetation strongly regulates surface O_3 through both chemical and physical pathways (Fowler et al., 2009; Monks et al., 2015; Clifton et al., 2020). Vegetation emits large amounts of biogenic volatile organic compounds (BVOC), particularly isoprene and monoterpenes, which are important precursors of tropospheric O_3 and secondary organic aerosols (Trainer et al., 1987; Chameides et al., 1988). These emissions far exceed anthropogenic non-methane VOC sources globally and represent a dominant source of reactive carbon in the atmosphere (Guenther et al., 1995; Guenther et al., 2012; Sindelarova et al., 2014), strongly enhancing O_3 formation in NO_x-rich environment (Chameides et al., 1988; Fiore et al., 2005; Li et al., 2019). Meanwhile, vegetation acts as an important sink for O_3 through dry deposition (Wesely, 2007; Fowler et al., 2009; Clifton et al., 2020), which is controlled by leaf area, canopy structure, and stomatal conductance (Emberson et al., 2000; Fowler et al., 2009; Clifton et al., 2020). Once taken up, O_3 induces oxidative stress that suppresses photosynthesis, reduces stomatal conductance, and ultimately decreases ecosystem productivity (Sitch et al., 2007; Lombardozzi et al., 2015; Yue et al., 2015), forming a two-way land-atmosphere coupling.

The representation of O_3-vegetation interactions in Earth system models (ESMs) has evolved substantially. Early land surface models focused on energy, water, and momentum exchanges, neglecting biogeochemical and chemical feedbacks (Bonan, 1995; Sellers et al., 1996; Pitman, 2003). The development of Dynamic Global Vegetation Models (DGVMs), such as IBIS, LPJ, and TRIFFID, enabled the explicit representation of vegetation dynamics and carbon cycling (Foley et al., 1996; Cox, 2001; Sitch et al., 2003). Thereafter, BVOC emission modules were implemented

https://doi.org/10.5194/egusphere-2026-4387
Preprint. Discussion started: 17 August 2026

into DGVMs to enable quantitative assessment of vegetation-driven impacts on atmospheric chemistry (Guenther et al., 2006; Arneth et al., 2007). More recently, ESMs have incorporated O_3 dry deposition and vegetation damage processes, allowing assessments of O_3 impacts on photosynthesis and carbon uptake (Lombardozzi et al., 2015; Yue and Unger, 2015).

Despite these advances, fully coupled O_3-vegetation interactions remain inadequately represented in current ESMs. In most models, BVOC emissions and O_3 dry deposition are included, but O_3 damage to vegetation is either absent or implemented using prescribed O_3 concentrations and empirical parameterizations. Consequently, O_3 impacts on vegetation and their feedbacks on atmospheric chemistry are typically treated separately rather than within a unified dynamic system, preventing a fully two-way feedback. To address this limitation, we couple the ECHAM6.3-HAM2.3-MOZ1.0 ESM with the interactive Model for Air Pollution and Land Ecosystems (iMAPLE). Within this framework, O_3-vegetation coupling is incorporated via three major pathways: (1) BVOC emissions that affect O_3 formation; (2) vegetation-mediated O_3 dry deposition; and (3) O_3-induced vegetation damage. Through a series of sensitivity experiments, we quantify the individual contributions of these processes to surface O_3 concentrations at global and regional scales, with emphasis on polluted areas such as eastern Asia and North America.

2. Methods and data

2.1 Models

The ESM used in this study is ECHAM6.3-HAM2.3-MOZ1.0 (hereafter ECHAM-HAMMOZ), which was jointly developed by the Max Planck Institute for Meteorology and several collaborating institutions (Schultz et al., 2018). ECHAM-HAMMOZ couples a comprehensive atmospheric general circulation model with interactive aerosol and atmospheric chemistry modules, enabling the simulation of coupled meteorological, chemical, and aerosol processes from regional to global scales (Schultz et al., 2018). ECHAM6.3 provides the atmospheric dynamical core and physical framework, simulating large-scale circulation and key physical processes including radiative transfer, cloud microphysics, convection, turbulence, and land-atmosphere exchanges (Stevens et al., 2013). HAM2.3 is an aerosol module that considers the emission, transport, chemical transformation, and removal of major species, including sulfate, black carbon, organic carbon, sea salt, and mineral dust, as well as their interactions with radiation and cloud (Stier et al., 2005; Zhang et al., 2012). MOZ1.0 is developed based on the MOZART chemistry mechanism, with detailed tropospheric and lower-stratospheric chemistry including the oxidation of VOCs, nitrogen oxides (NO_x), and O_3, thereby enabling the simulation of atmospheric oxidizing capacity and O_3 formation processes (Kinnison et al., 2007; Emmons et al., 2010).

iMAPLE is a process-based land surface model considering both vegetation dynamics and key biogeochemical processes (Yue and Unger, 2015; Yue et al., 2024). It provides a comprehensive representation of terrestrial ecosystem processes, including vegetation physiology, plant growth, and carbon allocation. The model is specifically designed to resolve interactions between air pollution and ecosystem functioning. For example, iMAPLE employs a photosynthesis-based BVOC emission scheme (PS_BVOC) to predict emissions of isoprene and monoterpene (Yue and Unger, 2015). It also includes an O_3 damage parameterization that quantifies the effects of O_3 exposure on leaf-level photosynthesis and vegetation productivity through stomatal uptake (Yue and Unger, 2015).

2.2 O_3-vegetation coupling

By incorporating iMAPLE into ECHAM-HAMMOZ, we establish a coupled model (ECHAM-HAMMOZ-iMAPLE, short as ECHAM-Hi thereafter) to represent O_3-vegetation interactions (Figure 1), in which vegetation modulates O_3 levels through biogenic emissions and dry deposition, while O_3 in turn impairs vegetation physiology via stomatal uptake.

https://doi.org/10.5194/egusphere-2026-4387
Preprint. Discussion started: 17 August 2026

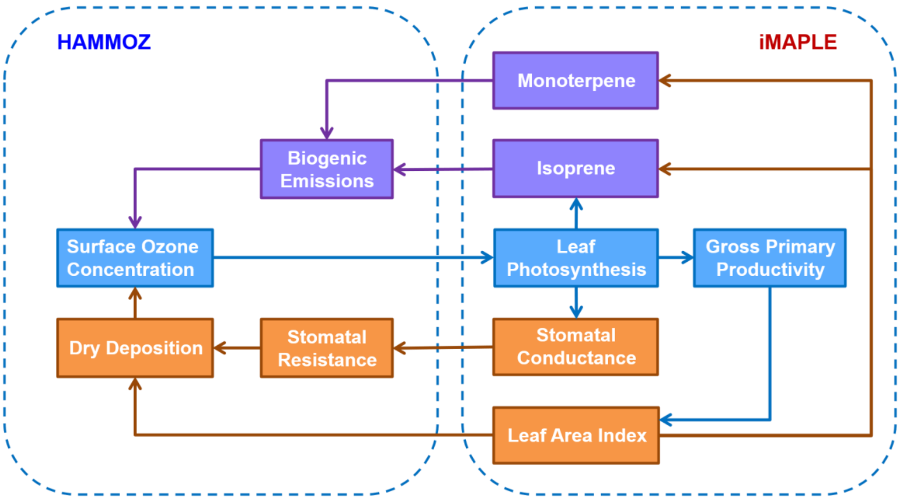

Figure 1. Schematic plot of the interactions between ecosystem and atmospheric chemistry in ECHAM-HAMMOZ-iMAPLE (short as ECHAM-Hi)

2.2.1 Biogenic emissions

The original HAMMOZ module applies prescribed biogenic emissions. Here, we use iMAPLE to dynamically simulate emissions of isoprene and monoterpenes, the two dominant BVOC species. Isoprene emissions are simulated using the PS_BVOC scheme to link with leaf photosynthetic activity (Unger et al., 2013) :

$$E_I = J_e \cdot \beta \cdot \kappa_p \cdot \tau \cdot \varepsilon, \qquad (1)$$

where E_I is the isoprene emission rate (μmol m^{-2} [leaf] s^{-1}), and J_e is the electron transport-limited photosynthetic rate (μmol m^{-2} [leaf] s^{-1}). The β converts electron flux into isoprene equivalents. The factor κ_p represents the inhibitory effect of atmospheric CO_2 on isoprene production, while τ accounts for differences in the temperature optima of photosynthesis and isoprene synthase activity. The ε denotes the plant functional type (PFT) specific fraction of electrons available for isoprene synthesis, also referred to as the isoprene emission potential.

Monoterpene emissions are simulated using a simplified temperature-dependent algorithm following Lathière et al. (2006). The leaf-level monoterpene emission rate (E_M, μmol m^{-2} [leaf] s^{-1}) is calculated as:

$$E_M = E_f \cdot C_T \cdot \kappa_p, \qquad (2)$$

https://doi.org/10.5194/egusphere-2026-4387
Preprint. Discussion started: 17 August 2026

where E_f is the PFT-specific emission factor based on Guenther et al. (1995). C_T is the temperature response factor. The same CO_2 inhibitory factor κ_p used for isoprene emissions is applied to monoterpenes. Simulated BVOC emissions are integrated with leaf area index (LAI) and passed online to HAMMOZ, where they participate in atmospheric oxidation chemistry and contribute to tropospheric O_3 formation.

2.2.2 Dry deposition

HAMMOZ computes O_3 dry deposition velocity using the Wesely (1989) scheme, in which stomatal resistance is parameterized as an empirical function of solar radiation and air temperature. Here, we replace the empirically derived stomatal resistance (s m^{-1}) with the reciprocal of dynamically predicted leaf stomatal conductance (g_s, m s^{-1}) from iMAPLE, in which g_s is calculated using the Ball-Berry scheme (Ball et al., 1987) :

$$g_s = m \frac{A_{net}}{c_s} \mathrm{RH} + \mathrm{b}, \quad (3)$$

where A_{net} is net leaf photosynthesis (μmol m^{-2} [leaf] s^{-1}); c_s is CO_2 concentration at the leaf surface (μmol m^{-3}) ; RH is relative humidity; m is an empirical slope controlling the sensitivity of stomatal conductance to photosynthesis and is modified by plant water stress; b (m s^{-1}) represents the minimum stomatal conductance when A_{net} is 0.

We also update the LAI, which determines the effective leaf surface area available for O_3 dry deposition. In iMAPLE, LAI is calculated on a daily time scale as follows:

$$\mathrm{LAI} = f \cdot LAI_{max}, \quad (4)$$

where f is the phenological factor determined by meteorological conditions, and $LAI_{\max}$ represents the maximum attainable LAI, which is related to vegetation structural properties and carbon content (Cox, 2001; Clark et al., 2011). The modifications of both g_s and LAI jointly alter O_3 dry deposition velocity, thereby influencing near-surface O_3 concentrations.

2.2.3 O_3 vegetation damage

In iMAPLE, gross primary productivity (GPP) is calculated by vertically integrating the total leaf photosynthetic rate (A_{tot}, μmol m^{-2} [leaf] s^{-1}) across the canopy:

https://doi.org/10.5194/egusphere-2026-4387
Preprint. Discussion started: 17 August 2026

$$\mathrm{GPP} = \int_0^{LAI} A_{tot} dL. \quad (5)$$

A_{tot} is constrained by the most limiting of three processes: Rubisco carboxylation capacity, electron transport-limited RuBP regeneration, and product synthesis limitations associated with phosphate availability in C_3 plants or phosphoenolpyruvate regeneration in C_4 plants.

We consider the GPP reduction caused by stomatal O_3 uptake using the O_3 damage scheme proposed by Sitch et al. (2007), in which the O_3 damage factor F is parameterized as a function of stomatal O_3 flux:

$$\mathrm{F} = \begin{cases} -a\left(F_{O_3} - T_{O_3}\right), & F_{O_3} > T_{O_3} \\ 0, & F_{O_3} \le T_{O_3} \end{cases}, \quad (6)$$

where a is the PFT-specific O_3 damage sensitivity parameter, and T_{O_3} is the threshold stomatal O_3 flux (μmol m^{-2} s^{-1}). O_3 damage is assumed to occur only when stomatal O_3 uptake exceeds this threshold. The stomatal O_3 flux (F_{O_3}, μmol m^{-2} s^{-1}) is calculated as:

$$F_{O_3} = \frac{[O_3]}{r_a + r_b + k \cdot r_s}, \quad (7)$$

where $[O_3]$ is the O_3 concentration at the canopy top. r_a, r_b and r_s denote aerodynamic resistance, boundary-layer resistance, and stomatal resistance, respectively (s m^{-1}). The O_3-damaged photosynthetic rate (A_{totd}, μmol m^{-2} [leaf] s^{-1}) and stomatal conductance (g_{sd}, m s^{-1}) are calculated as:

$$A_{totd} = (1 + F) A_{tot}, \quad (8)$$

$$g_{sd} = (1 + F) g_s. \quad (9)$$

Reduced photosynthetic capacity subsequently alters GPP, which further affects downstream ecosystem variables, including BVOC emissions (isoprene and monoterpenes), LAI, and stomatal conductance. These changes feed back to atmospheric chemistry through both emission and deposition processes, thereby establishing the two-way coupling between atmosphere chemistry and terrestrial ecosystem (Figure 1).

2.3 Data

2.3.1 Emissions

Anthropogenic emissions were adopted from three inventories to ensure consistent long-term coverage and improved regional representation. Global emissions for 1990-2014 were obtained

https://doi.org/10.5194/egusphere-2026-4387
Preprint. Discussion started: 17 August 2026

from the Community Emissions Data System (CEDS), which provides global gridded emissions of reactive trace gases and aerosols (Hoesly et al., 2018). Emissions for 2015-2100 were obtained from the CMIP6 input4MIPs forcing dataset developed by Gidden et al. (2025), which provides standardized emissions and boundary conditions for CMIP6 climate model experiments. We adopted the SSP5-8.5 high-emission scenario generated by the IAMC-REMIND-MAGPIE integrated assessment model.

In China, anthropogenic emissions were replaced with the Multi-resolution Emission Inventory for China (MEIC v1.4), which provides high-resolution emission estimates tailored to China's socioeconomic and industrial conditions (Geng et al., 2024). MEIC is developed using a unified source classification framework and region-specific emission factors for China, integrating bottom-up statistical data, process-based modeling, and big-data-driven emission fusion techniques. Compared to global inventories, MEIC offers a more detailed representation of sectoral emissions and spatial heterogeneity over China, and has been extensively applied in regional air quality simulations, atmospheric chemistry studies, and policy assessments (Li et al., 2017).

2.3.2 Validations

LAI and GPP used for model validations were obtained from the Global Land Surface Satellite (GLASS) product (Liang et al., 2021). GLASS integrates multi-source satellite observations with ground measurements to provide long-term, high-quality global datasets for terrestrial ecosystem monitoring. In this study, we used the GPP product derived from the Advanced Very High Resolution Radiometer (AVHRR) and the LAI product retrieved from the Moderate Resolution Imaging Spectroradiometer (MODIS). The original 0.05° datasets were re-gridded to the model resolution of 1.875° and averaged for the period of 2013-2015 to facilitate the comparison.

Surface O_3 observations used for model evaluation comprised 4,016 monitoring sites across China, North America, and Europe during 2013–2015. Observations over China were obtained from the Air Quality Monitoring Network operated by the Ministry of Ecology and Environment (AQMN-MEE), which provides near-real-time, quality-controlled measurements widely used for air pollution assessment, atmospheric chemistry model evaluation, and environmental policy analysis. Surface O_3 data for North America and Europe were taken from Sofen et al. (2016), which

https://doi.org/10.5194/egusphere-2026-4387
Preprint. Discussion started: 17 August 2026

compiles approximately 2,200 quality-controlled monitoring sites, mainly in U.S. and Europe, with over 200 million valid records. Owing to its extensive spatial coverage and rigorous quality assurance, this dataset has been widely used for evaluating atmospheric chemistry models.

2.4 Experiments

To quantify the individual contributions of land-atmosphere interaction pathways to surface O_3 and ecosystem responses, we conducted a series of sensitivity experiments with progressively increasing model complexity (Table 1). A baseline simulation (Base) was firstly conducted without any interactive coupling between the atmospheric chemistry and terrestrial ecosystem components. Subsequent experiments then sequentially activated individual interaction pathways to isolate their effects on surface O_3. In Exp_isp, the isoprene emission pathway (ISP) was enabled, allowing isoprene emissions simulated by iMAPLE to affect atmospheric chemistry in HAMMOZ. Exp_mtp further activated the monoterpene emission pathway (MTP) to account for the combined effects of the two major BVOC sources on O_3 formation. Exp_lai additionally incorporated the LAI pathway, through which vegetation structural changes influence O_3 dry deposition by modifying the effective deposition surface area. Exp_gs activated the stomatal conductance (Gs) pathway, which regulates stomatal resistance and thereby controls O_3 uptake by vegetation. In Exp_all, surface O_3 simulated by HAMMOZ directly affects vegetation physiology through the O_3 damage scheme in iMAPLE. In turn, O_3-induced changes in vegetation state and function feed back to the atmosphere through both altered BVOC emissions and modified dry deposition. This stepwise design enables attribution of the incremental contribution of each process, isolating the effects of isoprene emissions, monoterpene emissions, LAI-driven deposition changes, stomatal regulation, and O_3 vegetation damage on surface O_3 and/or ecosystem productivity.

Table 1. Summary of sensitivity experiments

Experiment	Isoprene emissions	Monoterpene emissions	LAI in deposition	Stomatal conductance	O_3 vegetation damage
Base	NO	NO	NO	NO	NO
Exp_isp	YES	NO	NO	NO	NO
Exp_mtp	YES	YES	NO	NO	NO
Exp_lai	YES	YES	YES	NO	NO
Exp_gs	YES	YES	YES	YES	NO
Exp_all	YES	YES	YES	YES	YES

https://doi.org/10.5194/egusphere-2026-4387
Preprint. Discussion started: 17 August 2026

3 Results

3.1 Model evaluations

We evaluate simulated boreal summer (June-August) surface O_3, GPP, and LAI from ECHAM-Hi against observational datasets (Fig. 2). The model reproduces the observed spatial pattern of surface O_3 (Fig. 2a, d), with hotspots over eastern Asia, central North America, and eastern Europe, leading to a correlation coefficient (R) of 0.61, a root mean square error (RMSE) of 13.4 ppbv, and a relative mean bias (RMB) of 14.2% (Fig. 2g). Simulated GPP and LAI also agree well with satellite-based products. Globally, the simulated boreal summer total GPP is 41.2 Pg C, slightly lower the observed 43.2 Pg C, with an RMSE of 1.84 gC m^{-2} day^{-1}, an RMB of -2.58%, and an R of 0.79 (Fig. 2h). Simulated LAI exhibits a global mean of 1.01 m^2 m^{-2}, comparable to 1.14 m^2 m^{-2} from observations, with an RMSE of 0.89 m^2 m^{-2}, an RMB of -11.17%, and an R of 0.79 (Fig. 2i). Overall, ECHAM-Hi captures both the spatial distribution and magnitude of key atmospheric composition and ecosystem variables during boreal summer, indicating robust performance of the coupled system.

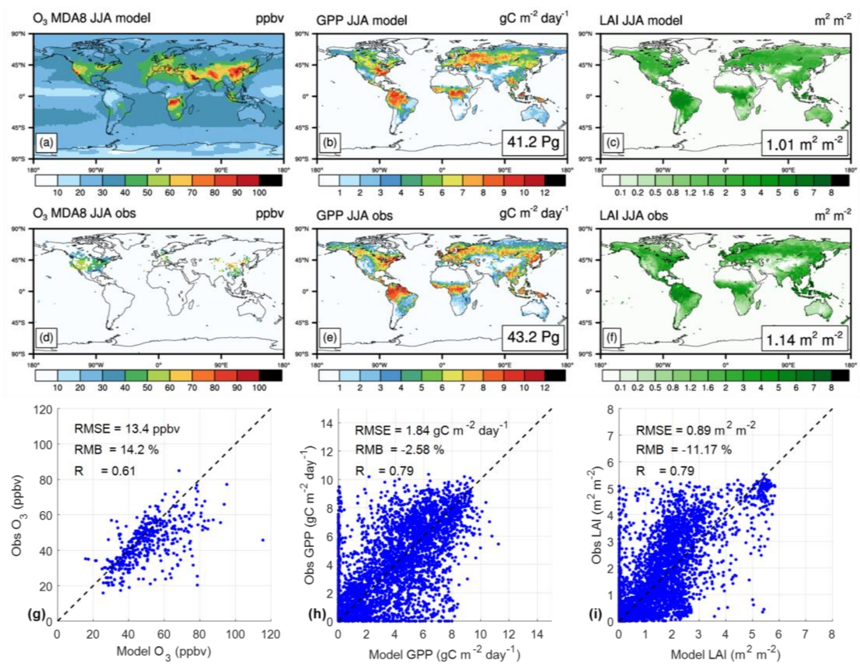

Figure 2. Evaluation of simulated (a) surface maximum daily 8-hour average (MDA8) ozone (O_3) concentrations, (b) gross primary productivity (GPP), and (c) leaf area index (LAI) against (d-f)

https://doi.org/10.5194/egusphere-2026-4387
Preprint. Discussion started: 17 August 2026

observations from (d) site-level measurements and (e, f) the GLASS data products for boreal summer (June–August) averaged over 2013-2015. Corresponding grid-level scatter plots are shown in (g-i), with correlation coefficient (R), relative mean bias (RMB), and root-mean-square error (RMSE) indicated.

3.2 Impacts of dynamic BVOC emissions on O_3

In the ECHAM-Hi model, the global isoprene emissions during boreal summer are 169.5 Tg (Fig. S1d), with a corresponding global mean surface O_3 concentration of 32.96 ppbv (Fig. S1b). Relative to the prescribed emissions in the original model (Fig. S1c), ECHAM-Hi simulates a 66.1 Tg (64.1%) increase in global isoprene emissions during boreal summer (Fig. 3b), with pronounced enhancements across the Northern Hemisphere (NH). This leads to heterogeneous changes in surface O_3, with increases primarily over land north of 45°N (Fig. 3a), particularly in East Asia (4–10 ppbv) and Europe (26 ppbv). In these regions, high anthropogenic NO_x emissions favor VOC-limited chemistry, whereby enhanced isoprene promotes O_3 formation. In contrast, O_3 decreases by 2–6 ppbv over large parts of North America and northern Asia, where NO_x levels are relatively low and chemistry is NO_x-limited; under these conditions, additional isoprene acts as a radical sink and suppresses O_3 production (Sillman, 1999; Fiore et al., 2005; Browne et al., 2013). Meanwhile, global monoterpene emissions increase by only 0.2 Tg (1.2%) reaching a total emission of 16.3 Tg (Fig. S2d), but exhibit pronounced spatial heterogeneity. Relative to the original model (Fig. S2c), ECHAM-Hi predicts substantial increases in high northern latitudes, while emissions decrease across most other regions (Fig. 3d). As a result, global surface O_3 shows widespread reductions (Fig. 3c), resulting from monoterpene enhancement in NO_x-limited regions but suppression in VOC-limited or warm regions.

https://doi.org/10.5194/egusphere-2026-4387
Preprint. Discussion started: 17 August 2026

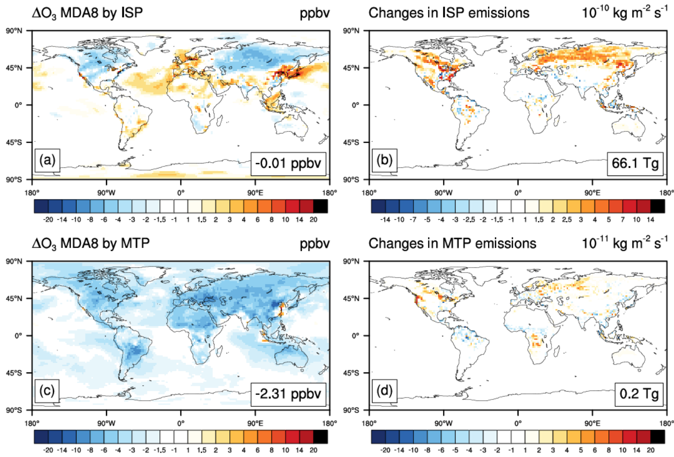

Figure 3. Changes of (a, c) surface MDA8 O_3 concentrations in response to changes in (b) isoprene (ISP) and (d) monoterpene (MTP) emissions averaged for the boreal summer (June–August) of 2013–2015.

3.3 Impacts of updated dry deposition on O_3

The dynamically simulated LAI from ECHAM-Hi is larger than the original model by 0.026 m^2 m^{-2} globally, reaching an average value of 1.035 m^2 m^{-2} (Fig. S3d), with pronounced increases in the northern high latitudes and tropical rainforests (Fig. 4b). In contrast, LAI decreases over middle latitudes in both hemispheres, especially in Asia and the Sahel. These LAI changes result in corresponding shifts in O_3 dry deposition velocity, with increases over boreal regions and the eastern U.S., but decreases over East Asia and northern Africa (Fig. 4c). As a result, global mean surface O_3 increases by 0.11 ppbv (Fig. 4a), exhibiting a spatial pattern broadly opposite to that of LAI. The LAI-induced reduction in dry deposition enhances surface O_3 by 3-8 ppbv over eastern China and by 2-4 ppbv over western Europe, thereby dominating the global mean positive response.

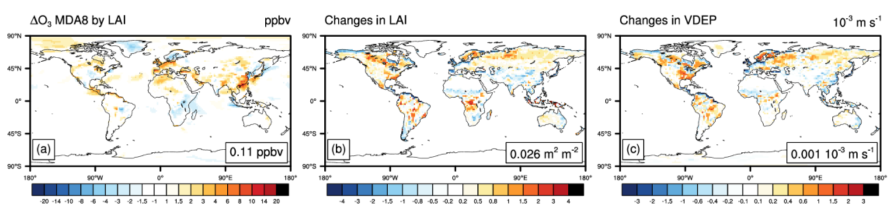

Figure 4. Changes of (a) surface MDA8 O_3 concentrations in response to (b) LAI changes and (c) LAI-induced changes in dry deposition velocity averaged for boreal summer (June–August) of 2013–2015.

Stomatal conductance simulated by iMAPLE was converted to leaf surface resistance and

https://doi.org/10.5194/egusphere-2026-4387
Preprint. Discussion started: 17 August 2026

coupled to the dry deposition in ECHAM-HAMMOZ (Fig. 5). Relative to the original leaf resistance (Fig. S4c), which in general has only the latitudinal gradient, the updated resistance better represents spatial variability across different land-cover types (Fig. S4d). As a result, the global mean leaf surface resistance increased by approximately 60 s m^{-1} (Fig. 5b). The largest increases occurred over deserts, plateaus, tundra, and ice-covered regions, where sparse vegetation and low canopy conductance produce high surface resistance. In contrast, densely vegetated regions, particularly eastern and southern Asia, exhibited decreases of up to 100 s m^{-1} in leaf surface resistance (Fig. 5b), leading to increases in O_3 dry deposition velocity of ~0.8×10^{-3} m s^{-1} (Fig. 5c). Consequently, surface O_3 concentrations decreased by ~3 ppbv over eastern Asia (Fig. 5a).

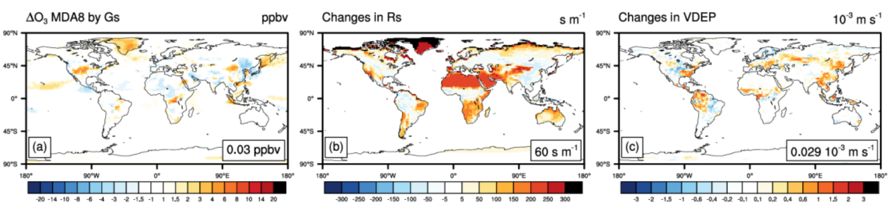

Figure 5. Changes of (a) surface MDA8 O_3 concentrations in response to (b) changed leaf resistance and (c) the associated changes in dry deposition velocity (VDEP) averaged for boreal summer (June–August) of 2013–2015.

3.4 O_3 vegetation damage (OVD) and feedback

OVD leads to a global GPP loss of 2.5 Pg C (5.7%) during boreal summer (Fig. 6). This reduction is slightly stronger than the estimate of 4.8% by Ma et al. (2023), likely because this study focuses on the boreal summer months when surface O_3 is usually at the peak. Regionally, high GPP losses of 1.6-3 gC m^{-2} day^{-1} occur over eastern China and U.S., where surface O_3 levels are usually high (Fig. 2a). When OVD feedback is activated, ECHAM-Hi predicts an even larger global GPP loss of 3.0 Pg C, with pronounced amplifications over eastern China and U.S. (Fig. 7a). This enhancement arises because initial O_3-induced photosynthesis loss suppresses LAI (Fig. 7b), which in turn decreases the total canopy GPP due to the reduction of leaf area (Equation 5).

https://doi.org/10.5194/egusphere-2026-4387
Preprint. Discussion started: 17 August 2026

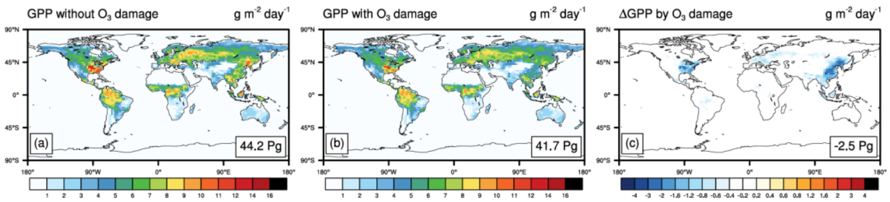

Figure 6. Simulation of (a) original GPP, (b) O_3-affected GPP, and (c) O_3-induced GPP loss (difference between a and b) averaged for boreal summer (June–August) of 2013–2015. The O_3-induced GPP loss does not feed back to affect vegetation growth.

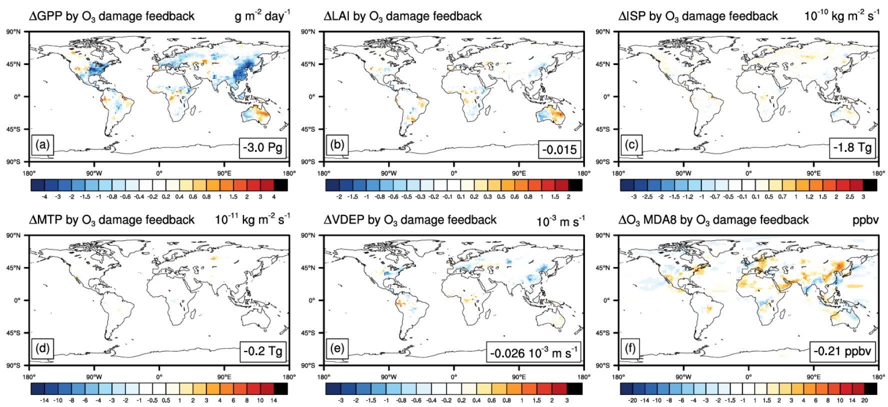

Figure 7. Responses of (a) GPP, (b) LAI, (c) ISP, (d) MTP, (e) VDEP, and (f) surface MDA8 O_3 to the online O_3 vegetation damaging effects during boreal summer (June–August) of 2013–2015.

The OVD feedback also influences atmospheric components. The LAI reduction leads to global decreases of 1.8 Tg C in isoprene emissions (Fig. 7c) and 0.2 Tg C in monoterpene emissions (Fig. 7d). Meanwhile, O_3-induced damages to stomatal conductance weakens O_3 dry deposition velocity (Fig. 7e), thereby increasing surface O_3 concentrations over eastern China, eastern U.S. and western Europe (Fig. 7f). This positive O_3 feedback is consistent with previous studies reporting similar O_3 enhancements using different models and/or vegetation damage schemes (Zhu et al., 2022; Cao et al., 2024). The online coupling also produces localized positive GPP responses (Fig. 7a), driven by reductions in surface O_3 associated with climate perturbations (Fig. 7f). As a result, LAI exhibits spatially heterogeneous changes, including patchy regional increases (Fig. 7b).

https://doi.org/10.5194/egusphere-2026-4387
Preprint. Discussion started: 17 August 2026

3.5 Feedback of O_3-vegetation coupling to surface O_3

Globally, O_3-vegetation coupling reduces the boreal summer mean surface O_3 concentration from 32.95 to 30.57 ppbv (-7.22%; Fig. 8a). Among the individual feedback pathways, ISP, MTP, and OVD decrease surface O_3, whereas LAI and Gs feedbacks increase it. The MTP pathway exerts the strongest influence, lowering the global mean surface O_3 by 2.31 ppbv (Fig. 8a), followed by the OVD pathway, which contributes a further 0.21 ppbv reduction. In contrast, ISP, LAI, and Gs show relatively modest net effects, reflecting spatially heterogeneous responses that largely offset each other at the global scale.

Regionally, O_3-vegetation coupling induces much larger perturbations. In East Asia, the mean boreal summer surface O_3 concentration increases by 1.33% from 79.82 to 80.88 ppbv (Fig. 8b). The ISP, LAI, and OVD pathways increase surface O_3 by 4.66, 3.53, and 1.51 ppbv, respectively. However, the MTP and Gs pathways on average reduce O_3 by 7.18 and 1.46 ppbv. In contrast, mean boreal summer surface O_3 over central North America decreases by 9.89%, from 52.95 to 47.71 ppbv (Fig. 8c). The LAI, Gs, and OVD pathways exert weaker influences than in East Asia, although their effects remain larger than the global mean. Here, changes in BVOC emissions dominate the O_3 response, with the MTP and ISP pathways reducing surface O_3 by 4.42 and 1.54 ppbv, respectively (Fig. 8c).

https://doi.org/10.5194/egusphere-2026-4387
Preprint. Discussion started: 17 August 2026

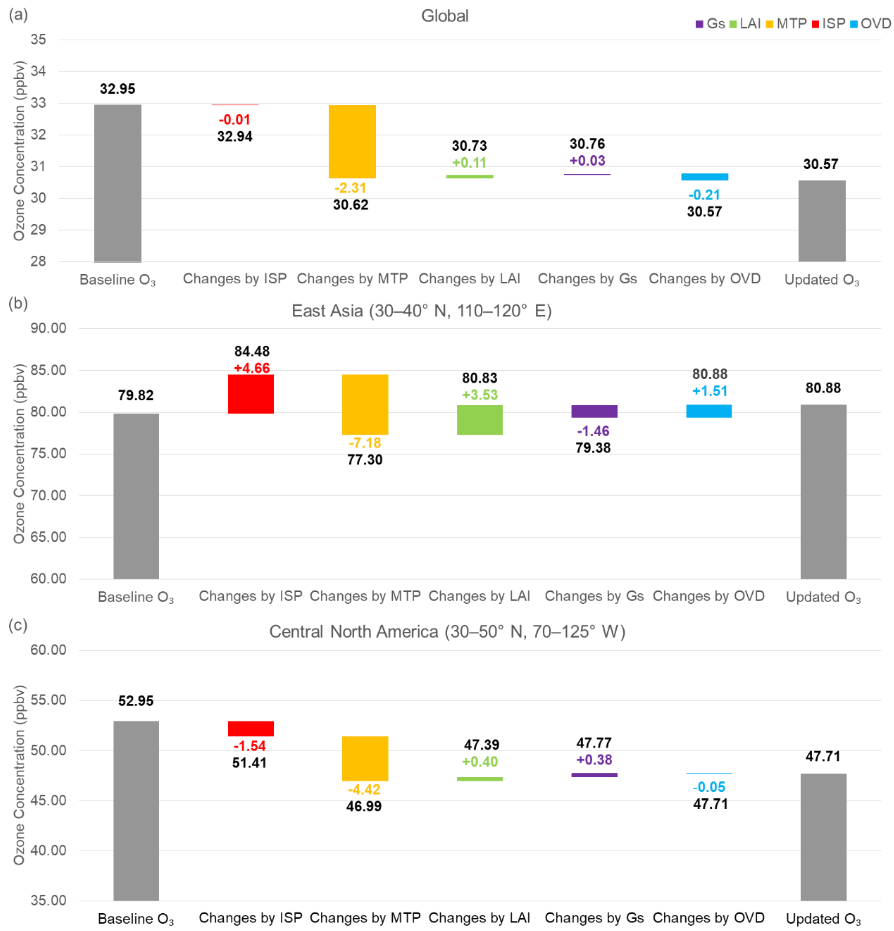

Figure 8. Changes in surface MDA8 O_3 concentrations attributable to individual processes included in the model development averaged over boreal summer (June–August) of 2013-2015 across (a) the globe, (b) East Asia, and (c) Northern Asia. OVD represents O_3 vegetation damage process.

4. Conclusions and discussion

In this study, we developed a fully coupled O_3-vegetation interaction framework by integrating the terrestrial ecosystem model iMAPLE into the ECHAM-HAMMOZ ESM. The coupled model explicitly represents three major land-atmosphere interaction pathways, including dynamic BVOC emissions, vegetation-mediated O_3 dry deposition, and O_3 damages to vegetation physiology. Incorporating these processes improve the simulation of surface O_3, particularly over China and the U.S. For example, the R between simulations and observations in China increases from 0.41 to 0.43,

https://doi.org/10.5194/egusphere-2026-4387
Preprint. Discussion started: 17 August 2026

while the RMSE decreases from 21.2 to 20.6 ppbv and the RMB from 31.5% to 29.7% (Fig. S5a, c). The improvement is more pronounced over the U.S., where the RMB declines from 19.0% to 7.8% and the RMSE from 10.7 to 9.5 ppbv (Fig. S5b, d), though the spatial R is weakened. Globally, O_3-vegetation coupling reduces the modeled O_3 levels (Fig. 5a), improving the originally positive biases against site-level measurements (Fig. 2g).

At the global scale, the updated ISP, LAI, and Gs exert limited impacts on surface O_3, either due to spatially heterogeneous changes relative to the original model (e.g., LAI and Gs) or compensating effects arising from nonlinear O_3 chemical sensitivity (e.g., ISP). For example, enhanced ISP in boreal regions decreases surface O_3, as additional BVOCs in NO_x-limited environments promotes O_3 chemical loss (Fiore et al., 2005; Browne et al., 2013). In contrast, the increased ISP in Asia supplies additional precursors for O_3 formation under VOC-limited conditions (Wu et al., 2020; Wang et al., 2023) , thereby enhancing surface O_3. The updated MTP produces the largest net effect, driven by consistent but opposing changes in BVOC emissions and chemical regimes. Over China, these responses are substantially amplified relative to the global means, likely because high anthropogenic NO_x emissions (Zheng et al., 2018) and elevated background O_3 (Wang et al., 2017) enhance the sensitivity of photochemical production to vegetation-driven changes in BVOC emissions and dry deposition. Overall, these results suggest that O_3-vegetation coupling can substantially modulate surface O_3 in chemically sensitive and/or highly vegetated regions.

Several limitations and uncertainties should be acknowledged. First, the evaluation of O_3 concentrations is constrained by the spatial coverage of available observations. In particular, monitoring sites remain sparse in regions such as Africa and Amazon, limiting a comprehensive assessment of model performance in these highly vegetated areas. Second, uncertainties remain in key process parameterizations, particularly in the representation of BVOC emissions and stomatal uptake responses to O_3 (Yue and Unger, 2015; Ma et al., 2023). Although the coupled model overall improves O_3 simulations, limited evaluations of BVOC emissions and stomatal conductance may influence the magnitude and spatial pattern of simulated O_3-vegetation feedbacks, leading to model-dependent quantifications. Third, although the coupled ECHAM-Hi model is capable of representing climate-chemistry-ecosystem interactions, this research mainly focuses on O_3-vegetation feedbacks to atmospheric composition. Previous studies have shown that temperature,

https://doi.org/10.5194/egusphere-2026-4387
Preprint. Discussion started: 17 August 2026

radiation, and extreme events can strongly influence coupled O_3-vegetation dynamics (Fischer et al., 2007; Oikonomakis et al., 2018; Zhang et al., 2018; Lin et al., 2020). Future work should incorporate these climatic feedbacks to further improve understanding of how climate change modulates ecosystem-atmosphere interactions and future air pollution.

Despite these limitations, this study highlights the importance of explicitly representing O_3–vegetation coupling in ESMs for accurately simulating surface O_3 and its regional impacts. By introducing process-based updates to BVOC emissions, dry deposition, and stomatal uptake, the model reveals that vegetation feedbacks can substantially modify surface O_3 with pronounced regional effects. These impacts are strongly amplified in chemically sensitive and highly polluted regions such as East Asia, while cleaner regions respond differently depending on chemical regimes. Overall, this work underscores that neglecting dynamic ecosystem–atmosphere interactions may lead to systematic biases in O_3 simulations, and that future projections of air quality and ecosystem health should account for coupled climate-chemistry-ecosystem feedbacks.

Data availability

Anthropogenic emissions of reactive gases and aerosols are adopted from the CEDS and CMIP6 input4mips datasets (https://metagrid.esgf-west.org/search, last access: 16 June 2026). For China, anthropogenic emissions are obtained from the MEIC inventory (http://meicmodel.org.cn/?page_id=541&lang=en, last access: 16 June 2026). Surface O_3 observations in North America and Europe used in this study are obtained from Sofen et al. (2016) (doi:10.5285/08fbe63d-fa6d-4a7a-b952-5932e3ab0452, last access: 16 June 2026). LAI and GPP observational datasets are obtained from Global land surface satellite products (GLASS, http://glass-product.bnu.edu.cn/englishpage.html, last access: 16 June 2026). The code and simulation data of the coupled model ECHAM-HAMMOZ-iMAPLE, as well as the surface O_3 observations in China, are available at https://doi.org/10.6084/m9.figshare.33263793.

Author contributions

XY conceived this research, reviewed and edited the manuscript. YZ established the bidirectional

https://doi.org/10.5194/egusphere-2026-4387
Preprint. Discussion started: 17 August 2026

interaction processes, designed the experiments, analyzed the data and wrote the draft paper. WF and CT helped with the modeling codes and paper revisions. JH and YH offered suggestions for model development.

Competing interests

The contact author has declared that none of the authors has any competing interests.

Acknowledgements

The authors thank the technical support of the National Large Scientific and Technological Infrastructure “Earth System Numerical Simulation Facility” (https://cstr.cn/31134.02.EL, last access: 16 June 2026).

Financial support

This research has been supported by the National Natural Science Foundation of China (42525503)， the National Key Research and Development Program of China (grant no. 2023YFF0805402) and Postgraduate Research & Practice Innovation Program of Jiangsu Province (Natural Science Program).

References

Anenberg, S. C., Horowitz, L. W., Tong, D. Q., and West, J. J.: An estimate of the global burden of anthropogenic ozone and fine particulate matter on premature human mortality using atmospheric modeling, Environ. Health Perspect., 118, 1189–1195, https://doi.org/10.1289/ehp.0901220, 2010.

Arneth, A., Niinemets, Ü., Pressley, S., Bäck, J., Hari, P., Karl, T., Noe, S., Prentice, I. C., Serça, D., Hickler, T., Wolf, A., and and Smith, B.: Process-based estimates of terrestrial ecosystem isoprene emissions: incorporating the effects of a direct CO2-isoprene interaction, Atmos. Chem. Phys., 7, 31–53, https://doi.org/10.5194/acp-7-31-2007, 2007.

Ball, J. T., Woodrow, I. E., and Berry, J. A.: A Model Predicting Stomatal Conductance and its Contribution to the Control of Photosynthesis under Different Environmental Conditions, in: Progress in Photosynthesis Research: Volume 4 Proceedings of the VIIth International Congress

https://doi.org/10.5194/egusphere-2026-4387
Preprint. Discussion started: 17 August 2026

on Photosynthesis Providence, Rhode Island, USA, August 10–15, 1986, edited by: Biggins, J., Springer Netherlands, Dordrecht, 221–224, https://doi.org/10.1007/978-94-017-0519-6_48, 1987.

Bonan, G. B.: Land-atmosphere CO2 exchange simulated by a land surface process model coupled to an atmospheric general circulation model, J. Geophys. Res.: Atmos., 100, 2817–2831, https://doi.org/10.1029/94JD02961, 1995.

Browne, E. C., Min, K. E., Wooldridge, P. J., Apel, E., Blake, D. R., Brune, W. H., Cantrell, C. A., Cubison, M. J., Diskin, G. S., Jimenez, J. L., Weinheimer, A. J., Wennberg, P. O., Wisthaler, A., and Cohen, R. C.: Observations of total RONO2 over the boreal forest: NOx sinks and HNO3 sources, Atmos. Chem. Phys., 13, 4543–4562, https://doi.org/10.5194/acp-13-4543-2013, 2013.

Cao, J., Yue, X., and Ma, M.: Simulation of ozone–vegetation coupling and feedback in China using multiple ozone damage schemes, Atmos. Chem. Phys., 24, 3973–3987, https://doi.org/10.5194/acp-24-3973-2024, 2024.

Chameides, W. L., Lindsay, R. W., Richardson, J., and Kiang, C. S.: The Role of Biogenic Hydrocarbons in Urban Photochemical Smog: Atlanta as a Case Study, Science, 241, 1473–1475, https://doi.org/10.1126/science.3420404, 1988.

Clark, D. B., Mercado, L. M., Sitch, S., Jones, C. D., Gedney, N., Best, M. J., Pryor, M., Rooney, G. G., Essery, R. L. H., Blyth, E., Boucher, O., Harding, R. J., Huntingford, C., and Cox, P. M.: The Joint UK Land Environment Simulator (JULES), model description – Part 2: Carbon fluxes and vegetation dynamics, Geosci. Model Dev., 4, 701–722, https://doi.org/10.5194/gmd-4-701-2011, 2011.

Clifton, O. E., Fiore, A. M., Massman, W. J., Baublitz, C. B., Coyle, M., Emberson, L., Fares, S., Farmer, D. K., Gentine, P., Gerosa, G., Guenther, A. B., Helmig, D., Lombardozzi, D. L., Munger, J. W., Patton, E. G., Pusede, S. E., Schwede, D. B., Silva, S. J., Sörgel, M., Steiner, A. L., and Tai, A. P. K.: Dry Deposition of Ozone Over Land: Processes, Measurement, and Modeling, Rev. Geophys., 58, e2019RG000670, https://doi.org/10.1029/2019RG000670, 2020.

Cooper, O. R., Parrish, D. D., Ziemke, J., Balashov, N. V., Cupeiro, M., and Galbally, I. E.: Global distribution and trends of tropospheric ozone: An observation-based review, Elem. Sci. Anth., 2, 000029, https://doi.org/10.12952/journal.elementa.000029, 2014.

Cox, P. M.: Description of the "TRIFFID" Dynamic Global Vegetation Model, Hadley Centre technical note 24, Hadley Centre, Met Office, London Road, Bracknell, Berks, RG122SY, UK， https://www.paleo.bristol.ac.uk/UM_Docs/UM_Technical_Documents/HCTN_24_TRIFFID.pdf2001.

Emberson, L. D., Ashmore, M. R., Cambridge, H. M., Simpson, D., and Tuovinen, J. P.: Modelling stomatal ozone flux across Europe, Environ. Pollut., 109, 403–413, https://doi.org/10.1016/S0269-7491(00)00043-9, 2000.

Emmons, L. K., Apel, E. C., Lamarque, J.-F., Hess, P. G., Avery, M., Blake, D., Brune, W., Campos, T., Crawford, J., DeCarlo, P. F., Hall, S., Heikes, B., Holloway, J., Jimenez, J. L., Knapp, D. J., Kok, G., Mena-Carrasco, M., Olson, J., O'Sullivan, D., Sachse, G., Walega, J., Weibring, P., Weinheimer, A., and Wiedinmyer, C.: Impact of Mexico City emissions on regional air quality from MOZART-4 simulations, Atmos. Chem. Phys., 10, 6195–6212, https://doi.org/10.5194/acp-10-6195-2010, 2010.

Fiore, A. M., Jacob, D. J., Field, B. D., Streets, D. G., Fernandes, S. D., and Jang, C.: Linking ozone pollution and climate change: The case for controlling methane, Geophys. Res. Lett., 29, 25-

21–25-24, https://doi.org/10.1029/2002gl015601, 2002.

Fiore, A. M., Horowitz, L. W., Purves, D. W., Levy II, H., Evans, M. J., Wang, Y., Li, Q., and Yantosca, R. M.: Evaluating the contribution of changes in isoprene emissions to surface ozone trends over the eastern United States, J. Geophys. Res.: Atmos., 110, https://doi.org/10.1029/2004JD005485, 2005.

Fischer, E. M., Seneviratne, S. I., Lüthi, D., and Schär, C.: Contribution of land-atmosphere coupling to recent European summer heat waves, Geophys. Res. Lett., 34, https://doi.org/10.1029/2006GL029068, 2007.

Foley, J. A., Prentice, I. C., Ramankutty, N., Levis, S., Pollard, D., Sitch, S., and Haxeltine, A.: An integrated biosphere model of land surface processes, terrestrial carbon balance, and vegetation dynamics, Global Biogeochem. Cycles, 10, 603–628, https://doi.org/10.1029/96GB02692, 1996.

Fowler, D., Pilegaard, K., Sutton, M. A., Ambus, P., Raivonen, M., Duyzer, J., Simpson, D., Fagerli, H., Fuzzi, S., Schjoerring, J. K., Granier, C., Neftel, A., Isaksen, I. S. A., Laj, P., Maione, M., Monks, P. S., Burkhardt, J., Daemmgen, U., Neirynck, J., Personne, E., Wichink-Kruit, R., Butterbach-Bahl, K., Flechard, C., Tuovinen, J. P., Coyle, M., Gerosa, G., Loubet, B., Altimir, N., Gruenhage, L., Ammann, C., Cieslik, S., Paoletti, E., Mikkelsen, T. N., Ro-Poulsen, H., Cellier, P., Cape, J. N., Horváth, L., Loreto, F., Niinemets, Ü., Palmer, P. I., Rinne, J., Misztal, P., Nemitz, E., Nilsson, D., Pryor, S., Gallagher, M. W., Vesala, T., Skiba, U., Brüggemann, N., Zechmeister-Boltenstern, S., Williams, J., O'Dowd, C., Facchini, M. C., de Leeuw, G., Flossman, A., Chaumerliac, N., and Erisman, J. W.: Atmospheric composition change: Ecosystems–Atmosphere interactions, Atmos. Environ., 43, 5193–5267, https://doi.org/10.1016/j.atmosenv.2009.07.068, 2009.

Gaudel, A., Cooper, O. R., and Ancellet, G.: Tropospheric Ozone Assessment Report: Present-day distribution and trends of tropospheric ozone relevant to climate and global atmospheric chemistry model evaluation, Elem. Sci. Anth., 6, 39, https://doi.org/10.1525/elementa.291, 2018.

Geng, G., Liu, Y., Liu, Y., Liu, S., Cheng, J., Yan, L., Wu, N., Hu, H., Tong, D., Zheng, B., Yin, Z., He, K., and Zhang, Q.: Efficacy of China's clean air actions to tackle PM2.5 pollution between 2013 and 2020, Nat. Geosci., 17, 987–994, https://doi.org/10.1038/s41561-024-01540-z, 2024.

Gidden, M., Riahi, K., Smith, S., Fujimori, S., Luderer, G., Kriegler, E., van Vuuren, D., van den Berg, M., Feng, L., Klein, D., Calvin, K., Doelman, J., Frank, S., Fricko, O., Harmsen, M., Hasegawa, T., Havlik, P., Hilaire, J., Hoesly, R., Horing, J., Popp, A., Stehfest, E., and Takahashi, K.: input4MIPs.CMIP6.ScenarioMIP.IAMC.IAMC-REMIND-MAGPIE-ssp585-1-1-supplemental-data, World Data Center for Climate (WDCC) at DKRZ [dataset], https://www.wdc-climate.de/ui/entry?acronym=I4M_5309664, 2025.

Guenther, A., Hewitt, C. N., Erickson, D., Fall, R., Geron, C., Graedel, T., Harley, P., Klinger, L., Lerdau, M., Mckay, W. A., Pierce, T., Scholes, B., Steinbrecher, R., Tallamraju, R., Taylor, J., and Zimmerman, P.: A global model of natural volatile organic compound emissions, J. Geophys. Res.: Atmos., 100, 8873–8892, https://doi.org/10.1029/94JD02950, 1995.

Guenther, A., Karl, T., Harley, P., Wiedinmyer, C., Palmer, P. I., and Geron, C.: Estimates of global terrestrial isoprene emissions using MEGAN (Model of Emissions of Gases and Aerosols from Nature), Atmos. Chem. Phys., 6, 3181–3210, https://doi.org/10.5194/acp-6-3181-2006, 2006.

Guenther, A. B., Jiang, X., Heald, C. L., Sakulyanontvittaya, T., Duhl, T., Emmons, L. K., and Wang, X.:

https://doi.org/10.5194/egusphere-2026-4387
Preprint. Discussion started: 17 August 2026

The Model of Emissions of Gases and Aerosols from Nature version 2.1 (MEGAN2.1): an extended and updated framework for modeling biogenic emissions, Geosci. Model Dev., 5, 1471–1492, https://doi.org/10.5194/gmd-5-1471-2012, 2012.

Hoesly, R. M., Smith, S. J., Feng, L., Klimont, Z., Janssens-Maenhout, G., Pitkanen, T., Seibert, J. J., Vu, L., Andres, R. J., Bolt, R. M., Bond, T. C., Dawidowski, L., Kholod, N., Kurokawa, J.-i., Li, M., Liu, L., Lu, Z., Moura, M. C. P., O'Rourke, P. R., and Zhang, Q.: Historical (1750–2014) anthropogenic emissions of reactive gases and aerosols from the Community Emissions Data System (CEDS), Geosci. Model Dev., 11, 369–408, https://doi.org/10.5194/gmd-11-369-2018, 2018.

IPCC: Climate Change 2021: The Physical Science Basis. Contribution of Working Group I to the Sixth Assessment Report of the IPCC, Cambridge University Press, Cambridge, https://doi.org/10.1017/9781009157896, 2021.

Kinnison, D. E., Brasseur, G. P., Walters, S., Garcia, R. R., Marsh, D. R., Sassi, F., Harvey, V. L., Randall, C. E., Emmons, L., Lamarque, J. F., Hess, P., Orlando, J. J., Tie, X. X., Randel, W., Pan, L. L., Gettelman, A., Granier, C., Diehl, T., Niemeier, U., and Simmons, A. J.: Sensitivity of chemical tracers to meteorological parameters in the MOZART-3 chemical transport model, J. Geophys. Res.: Atmos., 112, https://doi.org/10.1029/2006JD007879, 2007.

Lathière, J., Hauglustaine, D. A., Friend, A. D., De Noblet-Ducoudré, N., Viovy, N., and Folberth, G. A.: Impact of climate variability and land use changes on global biogenic volatile organic compound emissions, Atmos. Chem. Phys., 6, 2129–2146, https://doi.org/10.5194/acp-6-2129-2006, 2006.

Li, K., Jacob, D. J., Liao, H., Shen, L., Zhang, Q., and Bates, K. H.: Anthropogenic drivers of 2013–2017 trends in summer surface ozone in China, Proceedings of the National Academy of Sciences, 116, 422–427, https://doi.org/10.1073/pnas.1812168116, 2019.

Li, M., Liu, H., Geng, G., Hong, C., Liu, F., Song, Y., Tong, D., Zheng, B., Cui, H., Man, H., Zhang, Q., and He, K.: Anthropogenic emission inventories in China: a review, Natl. Sci. Rev., 4, 834–866, https://doi.org/10.1093/nsr/nwx150, 2017.

Liang, S., Cheng, J., Jia, K., Jiang, B., Liu, Q., Xiao, Z., Yao, Y., Yuan, W., Zhang, X., Zhao, X., and Zhou, J.: The Global Land Surface Satellite (GLASS) Product Suite, Bull. Am. Meteorol. Soc., 102, E323–E337, https://doi.org/10.1175/bams-d-18-0341.1, 2021.

Lin, M., Horowitz, L. W., Xie, Y., Paulot, F., Malyshev, S., Shevliakova, E., Finco, A., Gerosa, G., Kubistin, D., and Pilegaard, K.: Vegetation feedbacks during drought exacerbate ozone air pollution extremes in Europe, Nat. Clim. Change, 10, 444–451, https://doi.org/10.1038/s41558-020-0743-y, 2020.

Lombardozzi, D., Levis, S., Bonan, G., Hess, P. G., and Sparks, J. P.: The Influence of Chronic Ozone Exposure on Global Carbon and Water Cycles, J. Clim., 28, 292–305, https://doi.org/10.1175/JCLI-D-14-00223.1, 2015.

Lu, X., Zhang, L., Wang, X., Gao, M., Li, K., and Zhang, Y.: Severe surface ozone pollution in China: A global perspective, Environ. Sci. Technol. Lett., 5, 487–494, https://doi.org/10.1021/acs.estlett.8b00366, 2018.

Ma, Y., Yue, X., Sitch, S., Unger, N., Uddling, J., Mercado, L. M., Gong, C., Feng, Z., Yang, H., Zhou, H., Tian, C., Cao, Y., Lei, Y., Cheesman, A. W., Xu, Y., and Duran Rojas, M. C.: Implementation of trait-based ozone plant sensitivity in the Yale Interactive terrestrial Biosphere model v1.0 to assess global vegetation damage, Geosci. Model Dev., 16, 2261–2276,

https://doi.org/10.5194/egusphere-2026-4387
Preprint. Discussion started: 17 August 2026

https://doi.org/10.5194/gmd-16-2261-2023, 2023.

Mills, G., Pleijel, H., Malley, C. S., Sinha, B., Cooper, O. R., and Schultz, M. G.: Tropospheric Ozone Assessment Report: Present-day tropospheric ozone distribution and trends relevant to vegetation, Elem. Sci. Anth., 6, 47, https://doi.org/10.1525/elementa.302, 2018.

Monks, P. S., Archibald, A. T., Colette, A., Cooper, O., Coyle, M., Derwent, R., Fowler, D., Granier, C., Law, K. S., Mills, G. E., Stevenson, D. S., Tarasova, O., Thouret, V., von Schneidemesser, E., Sommariva, R., Wild, O., and Williams, M. L.: Tropospheric ozone and its precursors from the urban to the global scale from air quality to short-lived climate forcer, Atmos. Chem. Phys., 15, 8889–8973, https://doi.org/10.5194/acp-15-8889-2015, 2015.

Oikonomakis, E., Aksoyoglu, S., Wild, M., Ciarelli, G., Baltensperger, U., and Prévôt, A. S. H.: Solar "brightening" impact on summer surface ozone between 1990 and 2010 in Europe – a model sensitivity study of the influence of the aerosol–radiation interactions, Atmos. Chem. Phys., 18, 9741–9765, https://doi.org/10.5194/acp-18-9741-2018, 2018.

Pitman, A. J.: The evolution of, and revolution in, land surface schemes designed for climate models, Int. J. Climatol., 23, 479–510, https://doi.org/10.1002/joc.893, 2003.

Schultz, M. G., Stadtler, S., Schröder, S., Taraborrelli, D., Franco, B., Krefting, J., Henrot, A., Ferrachat, S., Lohmann, U., Neubauer, D., Siegenthaler-Le Drian, C., Wahl, S., Kokkola, H., Kühn, T., Rast, S., Schmidt, H., Stier, P., Kinnison, D., Tyndall, G. S., Orlando, J. J., and Wespes, C.: The chemistry–climate model ECHAM6.3-HAM2.3-MOZ1.0, Geosci. Model Dev., 11, 1695–1723, https://doi.org/10.5194/gmd-11-1695-2018, 2018.

Sellers, P. J., Randall, D. A., Collatz, G. J., Berry, J. A., Field, C. B., Dazlich, D. A., Zhang, C., Collelo, G. D., and Bounoua, L.: A Revised Land Surface Parameterization (SiB2) for Atmospheric GCMS. Part I: Model Formulation, J. Clim., 9, 676–705, https://doi.org/10.1175/1520-0442(1996)009<0676:ARLSPF>2.0.CO;2, 1996.

Sillman, S.: The relation between ozone, NOx and hydrocarbons in urban and polluted rural environments, Atmos. Environ., 33, 1821–1845, https://doi.org/10.1016/S1352-2310(98)00345-8, 1999.

Sindelarova, K., Granier, C., Bouarar, I., Guenther, A., Tilmes, S., Stavrakou, T., Müller, J. F., Kuhn, U., Stefani, P., and Knorr, W.: Global data set of biogenic VOC emissions calculated by the MEGAN model over the last 30 years, Atmos. Chem. Phys., 14, 9317–9341, https://doi.org/10.5194/acp-14-9317-2014, 2014.

Sitch, S., Smith, B., Prentice, I. C., Arneth, A., Bondeau, A., Cramer, W., Kaplan, J. O., Levis, S., Lucht, W., Sykes, M. T., Thonicke, K., and Venevsky, S.: Evaluation of ecosystem dynamics, plant geography and terrestrial carbon cycling in the LPJ dynamic global vegetation model, Global Change Biol., 9, 161-185, https://doi.org/10.1046/j.1365-2486.2003.00569.x, 2003.

Sitch, S., Cox, P. M., Collins, W. J., and Huntingford, C.: Indirect radiative forcing of climate change through ozone effects on the land-carbon sink, Nature, 448, 791–794, https://doi.org/10.1038/nature06059, 2007.

Sofen, E. D., Bowdalo, D., Evans, M. J., Apadula, F., Bonasoni, P., Cupeiro, M., Ellul, R., Galbally, I. E., Girgzdiene, R., Luppo, S., Mimouni, M., Nahas, A. C., Saliba, M., and Tørseth, K.: Gridded global surface ozone metrics for atmospheric chemistry model evaluation, Earth Syst. Sci. Data, 8, 41–59, https://doi.org/10.5194/essd-8-41-2016, 2016.

Stevens, B., Giorgetta, M., Esch, M., Mauritsen, T., Crueger, T., Rast, S., Salzmann, M., Schmidt, H., Bader, J., Block, K., Brokopf, R., Fast, I., Kinne, S., Kornblueh, L., Lohmann, U., Pincus, R.,

https://doi.org/10.5194/egusphere-2026-4387
Preprint. Discussion started: 17 August 2026

Reichler, T., and Roeckner, E.: Atmospheric component of the MPI-M Earth System Model: ECHAM6, J. Adv. Model. Earth Syst., 5, 146–172, https://doi.org/10.1002/jame.20015, 2013.

Stevenson, D. S., Young, P. J., Naik, V., Lamarque, J.-F., Shindell, D. T., and Voulgarakis, A.: Tropospheric ozone changes, radiative forcing and attribution to emissions in the Atmospheric Chemistry and Climate Model Intercomparison Project (ACCMIP), Atmos. Chem. Phys., 13, 3063–3085, https://doi.org/10.5194/acp-13-3063-2013, 2013.

Stier, P., Feichter, J., Kinne, S., Kloster, S., Vignati, E., Wilson, J., Ganzeveld, L., Tegen, I., Werner, M., Balkanski, Y., Schulz, M., Boucher, O., Minikin, A., and Petzold, A.: The aerosol-climate model ECHAM5-HAM, Atmos. Chem. Phys., 5, 1125–1156, https://doi.org/10.5194/acp-5-1125-2005, 2005.

Tai, A. P. K., Martin, M. V., and Heald, C. L.: Threat to future global food security from climate change and ozone air pollution, Nat. Clim. Change, 4, 817–821, 10.1038/nclimate2317, 2014.

Trainer, M., Williams, E. J., Parrish, D. D., Buhr, M. P., Allwine, E. J., Westberg, H. H., Fehsenfeld, F. C., and Liu, S. C.: Models and observations of the impact of natural hydrocarbons on rural ozone, Nature, 329, 705–707, https://doi.org/10.1038/329705a0, 1987.

Unger, N., Harper, K., Zheng, Y., Kiang, N. Y., Aleinov, I., Arneth, A., Schurgers, G., Amelynck, C., Goldstein, A., Guenther, A., Heinesch, B., Hewitt, C. N., Karl, T., Laffineur, Q., Langford, B., A. McKinney, K., Misztal, P., Potosnak, M., Rinne, J., Pressley, S., Schoon, N., and Serça, D.: Photosynthesis-dependent isoprene emission from leaf to planet in a global carbon-chemistry-climate model, Atmos. Chem. Phys., 13, 10243–10269, https://doi.org/10.5194/acp-13-10243-2013, 2013.

Wang, J., Zhang, Y., Xiao, S., Wu, Z., and Wang, X.: Ozone Formation at a Suburban Site in the Pearl River Delta Region, China: Role of Biogenic Volatile Organic Compounds, Atmosphere, 14, 609, https://doi.org/10.3390/atmos14040609, 2023.

Wang, T., Xue, L., Brimblecombe, P., Lam, Y. F., Li, L., and Zhang, L.: Ozone pollution in China: A review of concentrations, meteorological influences, chemical precursors, and effects, Sci. Total Environ., 575, 1582–1596, https://doi.org/10.1016/j.scitotenv.2016.10.081, 2017.

Wesely, M. L.: Parameterization of surface resistances to gaseous dry deposition in regional-scale numerical models, Atmospheric Environment (1967), 23, 1293–1304, https://doi.org/10.1016/0004-6981(89)90153-4, 1989.

Wesely, M. L.: Parameterization of surface resistances to gaseous dry deposition in regional-scale numerical models, Atmos. Environ., 41, 52–63, https://doi.org/10.1016/j.atmosenv.2007.10.058, 2007.

Wu, K., Yang, X., Chen, D., Gu, S., Lu, Y., Jiang, Q., Wang, K., Ou, Y., Qian, Y., Shao, P., and Lu, S.: Estimation of biogenic VOC emissions and their corresponding impact on ozone and secondary organic aerosol formation in China, Atmos. Res., 231, 104656, https://doi.org/10.1016/j.atmosres.2019.104656, 2020.

Young, P. J., Archibald, A. T., Bowman, K. W., Lamarque, J.-F., Naik, V., and Stevenson, D. S.: Pre-industrial to end 21st century projections of tropospheric ozone from the Atmospheric Chemistry and Climate Model Intercomparison Project (ACCMIP), Atmos. Chem. Phys., 13, 2063–2090, https://doi.org/10.5194/acp-13-2063-2013, 2013.

Yue, X. and Unger, N.: The Yale Interactive terrestrial Biosphere model version 1.0: description, evaluation and implementation into NASA GISS ModelE2, Geosci. Model Dev., 8, 2399–2417, https://doi.org/10.5194/gmd-8-2399-2015, 2015.

Yue, X., Unger, N., and Zheng, Y.: Distinguishing the drivers of trends in land carbon fluxes and plant volatile emissions over the past 3 decades, Atmos. Chem. Phys., 15, 11931–11948, https://doi.org/10.5194/acp-15-11931-2015, 2015.

Yue, X., Zhou, H., Tian, C., Ma, Y., Hu, Y., Gong, C., Zheng, H., and Liao, H.: Development and evaluation of the interactive Model for Air Pollution and Land Ecosystems (iMAPLE) version 1.0, Geosci. Model Dev., 17, 4621–4642, https://doi.org/10.5194/gmd-17-4621-2024, 2024.

Zhang, J., Gao, Y., Luo, K., Leung, L. R., Zhang, Y., Wang, K., and Fan, J.: Impacts of compound extreme weather events on ozone in the present and future, Atmos. Chem. Phys., 18, 9861–9877, https://doi.org/10.5194/acp-18-9861-2018, 2018.

Zhang, K., O'Donnell, D., Kazil, J., Stier, P., Kinne, S., Lohmann, U., Ferrachat, S., Croft, B., Quaas, J., Wan, H., Rast, S., and Feichter, J.: The global aerosol-climate model ECHAM-HAM, version 2: sensitivity to improvements in process representations, Atmos. Chem. Phys., 12, 8911–8949, https://doi.org/10.5194/acp-12-8911-2012, 2012.

Zheng, B., Tong, D., Li, M., Liu, F., Hong, C., Geng, G., Li, H., Li, X., Peng, L., Qi, J., Yan, L., Zhang, Y., Zhao, H., Zheng, Y., He, K., and Zhang, Q.: Trends in China's anthropogenic emissions since 2010 as the consequence of clean air actions, Atmos. Chem. Phys., 18, 14095–14111, https://doi.org/10.5194/acp-18-14095-2018, 2018.

Zhu, J., Tai, A. P. K., and Hung Lam Yim, S.: Effects of ozone–vegetation interactions on meteorology and air quality in China using a two-way coupled land–atmosphere model, Atmos. Chem. Phys., 22, 765–782, https://doi.org/10.5194/acp-22-765-2022, 2022.